Early View publication on www.interscience.wiley.com
(issue and page numbers not yet assigned;
citable using Digital Object Identifier – **DOI**)

phys. stat. sol. (b), 1–4 (2008) / **DOI** 10.1002/pssb.200743487

physica status solidi b
www.pss-b.com
basic solid state physics

Charge transport parameters of HBC at different temperatures

J. Kirkpatrick[*, 1, 2], V. Marcon[1], K. Kremer[1], J. Nelson[2], and D. Andrienko[1]

[1] Max Planck Institut für Polymerforschung, Ackermannweg 10, 55128 Mainz, Germany
[2] Department of Physics, Imperial College London, Prince Consort Road, London SW7 2BW, United Kingdom

Received 26 November 2007, accepted 17 January 2008
Published online 20 February 2008

PACS 64.70.mf, 72.20.Ee, 72.80.Le

[*] Corresponding author: e-mail james.kirkpatrick@mpip-mainz.mpg.de, Phone: +44 20 759 47 563, Fax: +44 20 759 42 077

We study the dependence on temperature of the charge transport parameters for hexabenzocoronene (HBC). Following from Marcus theory, two charge transport parameters will be calculated: the transfer integral and the difference in site energies. These parameters are strongly dependent on the orientation and position of molecules. Position and orientation of molecules are determined using molecular dynamics. Transfer integrals are calculated from a simplified INDO method. A technique to compute energetic disorder, that is the spread in site energies for the charge carriers, is developed. In the herringbone phase transfer integrals are higher, but so is energetic disorder. We consider three derivatives of HBC with different side chains, which lead to different phase behaviour and distributions of charge transport parameters.

© 2008 WILEY-VCH Verlag GmbH & Co. KGaA, Weinheim

1 Introduction Organic π-conjugated materials are used as active elements in electronic devices due to their semiconducting properties: field effect transistors, light emitting diodes, or solar cells. In all of these applications the efficiency of charge transport within organic layers plays a key role.

At high temperatures, the charge carriers are localised and the transport operates by a thermally activated hopping mechanism [1]. At the microscopic level, the charge transport can then be described as an electron (hole) transfer from a charged molecule to an adjacent neutral molecule. The hopping rate is given by Marcus expression

$$\omega_{ij} = \frac{|J_{ij}|^2}{\hbar}\sqrt{\frac{\pi}{\lambda kT}}\exp\left[-\frac{(\Delta G_{ij}-\lambda)^2}{4\lambda kT}\right]. \quad (1)$$

Equation (1) states that the key parameter for transport is the intermolecular transfer integral J_{ij}, that expresses the strength of electronic coupling. ΔG_{ij} represents the difference in free energies and determines the ratio of the rate of forward and backward hops. The reorganisation energy λ is a measure of electron–phonon coupling and introduces a temperature dependent prefactor for the charge transport.

The electronic coupling is proportional to wavefunction overlap and is very sensitive to the relative position and orientation of the molecules participating in charge transport. Hence, charge mobility is sensitive to the local ordering of molecules, presence of structural defects, and of course to the type of the mesophase.

The most common types of mesophases formed by discotic compounds are: (a) discotic nematic (ND), (b) hexagonal ordered (Dho), (c) hexagonal disordered (Dhd), (d, e, f) rectangular disordered with different plane group symmetry (Drd), (g) oblique (Dob), as shown in Fig. 1. In general, phases and phase transition temperatures are sensitive to side chains furnishing HBC core.

In this paper, we address the relation of the mesophase symmetry to the value of the charge transport parameters. Since the reorganisation energy is not strongly dependent on morphology we will not consider in this study.

2 Studied systems and computational method The molecular structures of the studied hexabenzocoronene derivatives are shown in Fig. 2. We considered three types of side chains: alkyl chains of length 12; branched 'dovetail' side chains, C_{10-6}; and dodecylphenyl-substituted PhC_{12} side chains. The choice of systems is based on our previous studies which show qualitatively different mesophase ordering [2] and, as a result, quantitatively different charge carrier mobilities [3]. In addition,

© 2008 WILEY-VCH Verlag GmbH & Co. KGaA, Weinheim

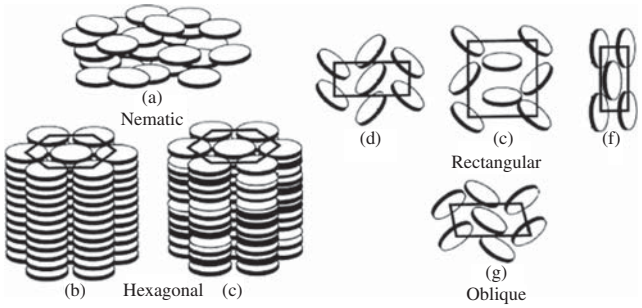

Figure 1 Types of common mesophases of discotic compounds.

these systems are well-characterised experimentally by various techniques: wide angle X-ray scattering, solid state NMR, and differential scanning calorimetry [4–9]. For charge transport pulse radiolysis time resolved microwave conductivity (PR-TRMC) data [4, 10] are also available. For some systems, time of flight measurements of mobility exist [11, 12].

2.1 Computation of electronic properties The charge transport parameters calculated are transfer integrals and site energy differences. Transfer integrals are calculated using an approximation of Zerner's semi-empirical Intermediate Neglect of Differential Overlap (INDO) [13]. Transfer integrals are calculated for closest intra-columnar neighbours, leading to two neighbours per molecule. Since the highest occupied and lowest unoccupied molecular orbitals (HOMO and LUMO) of HBC are doubly occupied, it is necessary to compute all four possible combinations of transfer integrals, (between HOMO and HOMO, HOMO and HOMO-1, HOMO-1 and HOMO, HOMO-1 and HOMO-1) and take the root mean square average [14].

The method used for calculating site energy differences is somewhat more novel. We assume that there are two main contributions to energetic disorder: an electrostatic contribution and a contribution due to polarisation effects. The importance of electrostatics has long been clear for charge transport in polar molecules dispersed in an inert matrix [15] and is also one of the mechanisms thanks to which long range correlations are assumed to occur in conjugated polymers [16, 17]. In the case of HBC, we want to be able to model the effect of both the local dipole moments between aromatic carbons and hydrogen atoms and the quadrupole moment due to the negative π electrons delocalised below and above the molecular plane. Of these two electric moments the first can be easily described by point charges located at each atomic position, but the second cannot. We therefore place a layer of point charges (ghost charges) at a distance above and below the carbons in the conjugated core of 0.47 Å [18]. DFT calculations of a neutral and charged molecule are then performed, and electrostatic charges are fitted to both the ghost atoms and normal atoms in the HBC core (ESP fitting). The MD simulation provides the position and orientation and hence site energies can easily be computed.

Polarisability has also been shown to be important in stabilising the energies of neutral and charged aromatic crystals [19]. In order to calculate site energy differences it is sufficient to know the difference in energy between a charged crystal with charge localised in a particular place rather than another, not the total interaction energy due to polarisation in the whole molecular crystal. In order to model this effect, we use a model of polarisable force field borrowed from the Ref. [20, 21]: we include polarisable point dipoles on each carbon atom on the HBC core. The polarisation of these atoms is determined from the external field (in our case caused by the point charges from ESP fitting), from the field from the induced dipoles and from the self energy of the dipoles. Such a problem is either solved self-consistently or via matrix inversion. Since we tend to work with systems with less than 2000 polarisable sites, we find matrix inversion more convenient computationally. Still, the fact that polarisation interactions are not pair-wise additive makes the computation of the polarisation contribution far more demanding. Following [20] we take a polarisability of 0.7 $Å^3$ with no cut-off radius for aromatic carbons.

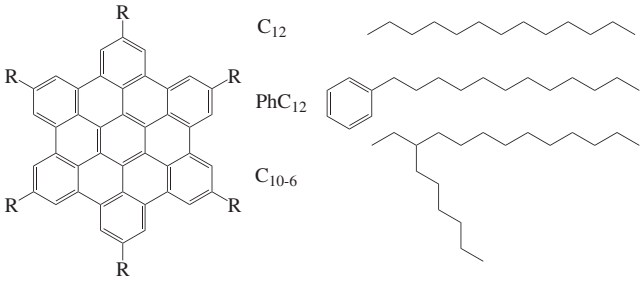

Figure 2 Studied derivatives of hexabenzocoronene.

2.2 Molecular dynamics Molecular dynamics simulations were performed with the parallel version of the GROMACS program [22]. We simulated systems of up to 320 molecules, arranged in columns of twenty molecules each. The initial configuration was either a herringbone (C_{12}, C_{10-6}) or hexagonal (PhC_{12}) arrangement of the columns. The distance between the columns and the molecules in the columns has been slightly increased to avoid site superposition. After the energy minimisation, a short equilibrating run (4 ns) was performed at a constant pressure $P = 0.1$ MPa, at different temperatures, using Parinello–Rahman barostat and Nose–Hoover thermostat. The simulation box angles where fixed at 90°. The electrostatic interactions were treated with the smooth particle-mesh Ewald (PME) method [23] (spacing for PME grid 0.12 nm, cutoff 0.9 nm). A time step of 2 fs was used to integrate equations of motion using the Velocity Verlet algorithm with 0.9 nm cutoff for short-range interactions. Bond lengths were constrained using LINCS algorithm [24]. The production run of 100 ns followed the initial equilibration of about 10 ns.

© 2008 WILEY-VCH Verlag GmbH & Co. KGaA, Weinheim

3 Results and discussion

3.1 Distribution of transfer integrals Figure 3 shows the variation with temperature of the standard deviation and mean in distribution of the logarithm of the effective transfer integral square for the C_{12} derivative. It is evident that temperature affects the transfer integral in two ways: upon a phase transition, the transfer integral is greatly reduced, within each phase the mean and distribution in transfer integral is largely left unchanged. The reduction of the mean of transfer integral is due to the different rotational alignment of molecules: in the crystalline phase, neighbouring molecules are on average in the same orientation, whereas in the liquid crystalline phase they tend to be rotated by 30° about the axis normal to the molecule with respect to each other. In the crystalline phase, neighbouring molecules are shifted with respect to each other, resulting in a tilt of the molecules with respect to the columnar axis. This leads to a reduction in molecular overlap. It seems from our calculations, that in the crystalline phase the increase in overlap due to better rotational register trumps the reduction due to shifting molecules over each other. It is also interesting to note that even though the width in the distribution of transfer integrals is always very similar, the distributions are slightly wider in the crystalline phase than in the liquid crystalline phase. In order to understand the existence of higher disorder in the crystalline phase we should bear in mind that in both phases the HBC cores are actually very well ordered and that the greatest change in order occurs in the side chains, rather than in the cores. In this case the distribution of transfer integrals is wider simply because the transfer integrals are greater. Within each phase, the distribution in transfer integrals becomes wider with temperature as a result of greater disorder.

Let us contrast the behaviour of transfer integrals in the C_{12} derivative, with the behaviour in the PhC_{12} derivative. The mean and standard deviation of the transfer integral are shown in Fig. 4. PhC_{12} does not display a phase transition and in fact the variation in its transfer integrals is much less pronounced. Curiously, in this case the variation in transfer integrals also becomes slightly narrower with increasing temperature.

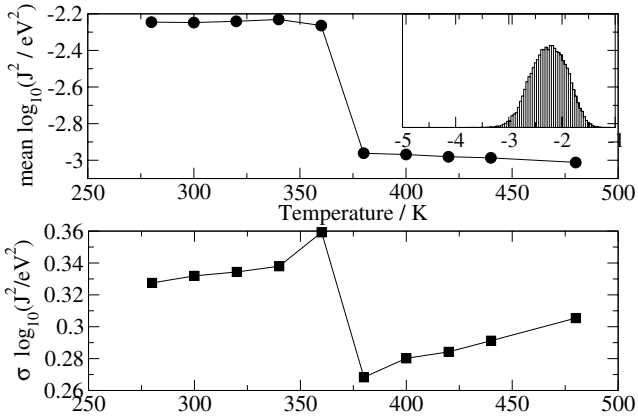

Figure 3 Average (circles) and standard deviation (squares) of the distribution of $\log(|J|^2)$ in eV for the C_{12} derivative. Inset: Distribution of $\log(|J|^2)$ in eV for the system at 300 °K.

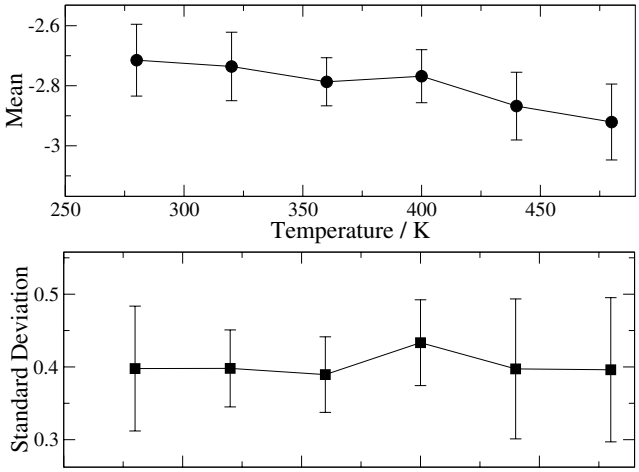

Figure 4 Average (circles) and standard deviation (squares) of the distribution of $\log(|J|^2)$ in eV for the PhC_{12} derivative.

Finally let us look at the variation in distribution of transfer integrals as a function of temperature for the dovetail derivative. Figure 5 shows the mean and standard deviation for the logarithm of the transfer integral square. In this case it appears that the mean falls sharply with temperature and that the standard deviation increases. What's more we can see strong deviation between the different columns (the error bars are large). In the insets to Fig. 5 the distribution of the $\log|J|^2$ at different temperature is shown. As the temperature is increased the median of transfer integrals squared is vastly increased, however we find that a large tail of low transfer integrals occurs. In other words,

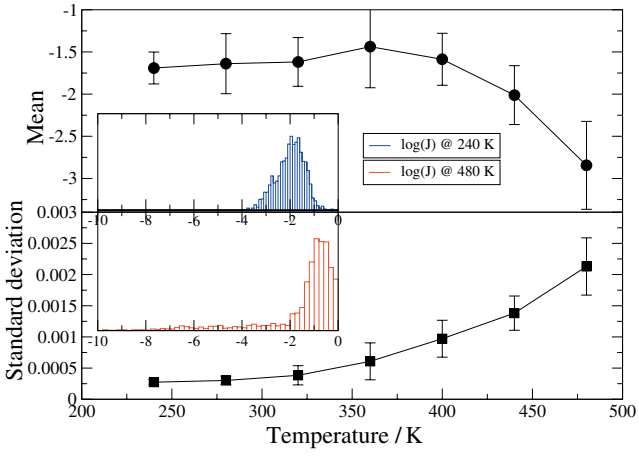

Figure 5 (online colour at: www.pss-b.com) Average (circles) and standard deviation (squares) of the distribution of $\log(|J|^2)$ in eV for the C_{10-6} dovetail derivative. Inset: Distribution of $\log(|J|^2)$ in eV for the system at 240 °K (blue bars) and at 480 °K (red bars).

© 2008 WILEY-VCH Verlag GmbH & Co. KGaA, Weinheim

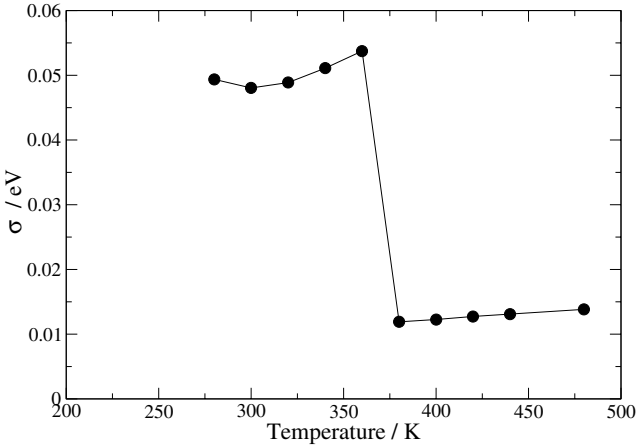

Figure 6 Standard deviation σ of the distribution of site energy difference for C_{12}.

when the columns break the square symmetry of the herringbone structure and get into an hexagonal structure, locally the discs pack discotically with very high transfer integrals, however these packets of well ordered molecules are misaligned and the transfer integrals between molecules on adjacent packets are very small.

3.2 Energetic disorder As explained in the Methods section, two different contributions to the energetic disorder have been considered: from electrostatic and polarisation effects. Both contributions to the distribution of site energy differences between nearest neighbours were calculated for two columns of C_{12}. Since we calculate site energies for each site at a particular MD snapshot relative to the electrostatic (and polarisation) energy of a neutral column, and since the energy of a neutral column is not going to be the same at all MD snapshots, we must always look at site energy *differences*. Polarisation reduces the distribution in site energy differences but always contributes less than 20% to the total width of the distribution.

Figure 6 shows the standard deviation σ of the distribution of site energy differences for C_{12} as a function of temperature. It can be seen that the phase transition is accompanied by a rather sharp decrease in energetic disorder. This effect is expected to somewhat reduce the difference in mobility before and after phase transition due to the variation in transfer integrals.

Acknowledgements This work was partially supported by DFG. V.M. acknowledges Alexander von Humboldt foundation. J.K. acknowledges the EPSRC.

References

[1] R. A. Marcus, Rev. Mod. Phys. **65**, 599 (1993).
[2] D. Andrienko, V. Marcon, and K. Kremer, J. Chem. Phys. **125**, 124902 (2006).
[3] J. Kirkpatrick, V. Marcon, J. Nelson, K. Kremer, and D. Andrienko, Phys. Rev. Lett. **98**, 227402 (2007).
[4] A. M. van de Craats, J. M. Warman, A. Fechtenkotter, J. D. Brand, M. A. Harbison, and K. Müllen, Adv. Mater. **11**, 1469 (1999).
[5] A. M. van de Craats, L. D. A. Siebbeles, I. Bleyl, D. Haarer, Y. A. Berlin, A. A. Zharikov, and J. M. Warman, J. Chem. Phys. **102**, 9625 (1998).
[6] I. Fischbach, T. Pakula, P. Minkin, A. Fechtenkötter, K. Müllen, H. W. Spiess, and K. Saalwächter, J. Phys. Chem. B **106**, 6408 (2002).
[7] P. Herwig, C. W. Kayser, K. Müllen, and H. W. Spiess, Adv. Mater. **8**, 510 (1996).
[8] S. P. Brown, I. Schnell, J. D. Brand, K. Müllen, and H. W. Spiess, J. Am. Chem. Soc. **121**, 6712 (1999).
[9] A. Fechtenkotter, K. Saalwachter, M. A. Harbison, K. Müllen, and H. W. Spiess, Angew. Chem. **38**, 3039 (1999).
[10] W. Pisula, M. Kastler, D. Wasserfallen, M. Mondeshki, J. Piris, I. Schnell, and K. Müllen, Chem. Mater. **18**, 3634 (2006).
[11] A. Rybak, J. Pfleger, J. Jung, M. Pavlik, I. Glowacki, J. Ulanski, Z. Tomovic, K. Müllen, and Y. Geerts, Synth. Met. **156**, 302 (2006).
[12] M. Kastler, F. Laquai, K. Müllen, and G. Wegner, Appl. Phys. Lett. **89**, 252103 (2006).
[13] J. Kirkpatrick, Int. J. Quantum Chem. **108**, 51–56 (2008).
[14] M. D. Newton, Chem. Rev. **91**, 767 (1991).
[15] P. M. Borsenberger and D. Weiss, Organic Photoreceptors for Xerography (Marcel Dekker, New York, 1998).
[16] S. V. Novikov and A. V. Vannikov, J. Phys. Chem. **99**, 14573 (1995).
[17] Y. N. Garstein and E. M. Conwell, Chem. Phys. Lett. **245**, 351 (1995).
[18] C. A. Hunter and J. K. M. Sanders, J. Am. Chem. Soc. **112**, 5525 (1990).
[19] E. V. Tsiper and Z. G. Soos, Phys. Rev. B, **64**, 195124 (2001).
[20] G. A. Kaminski, H. A. Stern, B. J. Berne, R. A. Friesner, Y. X. Cao, R. B. Murphy, R. Zhou, and T. A. Halgren, J. Comput. Chem. **23**, 1515 (2002).
[21] P. Ahlström, A. Wallqvist, A. Engström, and B. Jönsson, Mol. Phys. **68**, 563 (1989).
[22] E. Lindahl, B. Hess, and D. van der Spoel, J. Mol. Mod. **7**, 306 (2001).
[23] U. Essmann, L. Perera, M. L. Berkowitz, T. Darden, H. Lee, and L. G. Pedersen, J. Chem. Phys. **103**, 8577 (1995).
[24] B. Hess, H. Bekker, H. J. C. Berendsen, and J. G. E. M. Fraaije, J. Comput. Chem. **18**, 1463 (1997).

© 2008 WILEY-VCH Verlag GmbH & Co. KGaA, Weinheim